Received: 6 June 2022 | Revised: 31 August 2022 | Accepted: 2 September 2022

DOI: 10.1111/jsr.13733

RESEARCH ARTICLE

Automated real-time EEG sleep spindle detection for brain-state-dependent brain stimulation

Umair Hassan[1,2] | Gordon B. Feld[3] | Til Ole Bergmann[1,2,4]

[1]Neuroimaging Center (NIC), Focus Program Translational Neuroscience (FTN), Johannes Gutenberg University Medical Center, Mainz, Germany

[2]Leibniz Institute for Resilience Research, Mainz, Germany

[3]Department of Clinical Psychology, Central Institute of Mental Health, Medical Faculty Mannheim, Heidelberg University, Mannheim, Germany

[4]Department of Neurology & Stroke, Hertie Institute for Clinical Brain Research, Eberhard Karls University of Tübingen, Tübingen, Germany

Correspondence
Umair Hassan, Neuroimaging Center (NIC), Focus Program Translational Neuroscience (FTN), Johannes Gutenberg University Medical Center, Langenbeckstr. 1, 55131, Germany; Leibniz Institute for Resilience Research, Wallstraße 7-9, 55122, Mainz, Germany.
Email: umair.hassan@uni-mainz.de; umairhassankhanniazi@gmail.com

Funding information
Boehringer Ingelheim Foundation (BIF); German Research Foundation (DFG), Grant/Award Number: 362546008

Summary

Sleep spindles are a hallmark electroencephalographic feature of non-rapid eye movement sleep, and are believed to be instrumental for sleep-dependent memory reactivation and consolidation. However, direct proof of their causal relevance is hard to obtain, and our understanding of their immediate neurophysiological consequences is limited. To investigate their causal role, spindles need to be targeted in real-time with sensory or non-invasive brain-stimulation techniques. While fully automated offline detection algorithms are well established, spindle detection in real-time is highly challenging due to their spontaneous and transient nature. Here, we present the real-time spindle detector, a robust multi-channel electroencephalographic signal-processing algorithm that enables the automated triggering of stimulation during sleep spindles in a phase-specific manner. We validated the real-time spindle detection method by streaming pre-recorded sleep electroencephalographic datasets to a real-time computer system running a Simulink® Real-Time™ implementation of the algorithm. Sleep spindles were detected with high levels of Sensitivity (~83%), Precision (~78%) and a convincing F1-Score (~81%) in reference to state-of-the-art offline algorithms (which reached similar or lower levels when compared with each other), for both naps and full nights, and largely independent of sleep scoring information. Detected spindles were comparable in frequency, duration, amplitude and symmetry, and showed the typical time–frequency characteristics as well as a centro-parietal topography. Spindles were detected close to their centre and reliably at the predefined target phase. The real-time spindle detection algorithm therefore empowers researchers to target spindles during human sleep, and apply the stimulation method and experimental paradigm of their choice.

KEYWORDS
closed loop, electroencephalographic triggered stimulation, non-invasive brain stimulation, spindle cycle detection, spindle phase triggered, transcranial magnetic stimulation

1 | INTRODUCTION

Thalamocortical sleep spindles, i.e., 0.5–2-s bursts of oscillatory brain activity at sigma frequency (~12–15 Hz) with waxing and waning amplitude, are a hallmark feature of the electroencephalogram (EEG) during non-rapid eye movement (NREM) sleep. Spindles subserve sleep-dependent memory reactivation (Bergmann, Mölle, Diedrichs, et al., 2012) and systems consolidation (Diekelmann & Born, 2010) via their nested phase–amplitude coupling with neocortical slow oscillations (SOs; 0.5–1 Hz) and hippocampal ripples (> 80 Hz; Staresina

et al., 2015), supporting phase-dependent plasticity (Bergmann & Born, 2018) and the synaptic rescaling of cortical neurons (Klinzing et al., 2019). To investigate their neurophysiological underpinnings and test their causal role for memory consolidation, spindles need to be targeted and manipulated experimentally. In humans, non-invasive means such as the application of sensory or transcranial brain stimulation in a brain-state-dependent manner (Bergmann, 2018), as done successfully for the SO, provides an opportunity to interact directly with the electrophysiological brain activity of interest in a temporally and spatially precise fashion that cannot be achieved with more indirect, e.g., pharmacological, manipulations, the effects of which are more systemic and affect brain activity during longer time periods.

The SO phase-dependent transcranial magnetic stimulation (TMS) of the left human primary motor cortex (M1) during NREM sleep revealed that corticospinal excitability, as assessed by motor-evoked potentials (MEPs), were smaller during SO down- than up-states (Bergmann, Mölle, Schmidt, et al., 2012). Using closed-loop SO phase-triggered auditory stimulation, Ngo et al. (2013, 2015) were able to enhance SO amplitude, associated spindle generation and memory consolidation. Also, targeted memory reactivation studies successfully explored the benefit of targeting reactivation cues phase-locked to SO up- or down-states (Göldi et al., 2019; Shimizu et al., 2018).

While SOs are an easy real-time target, also faster oscillations can be targeted using modern real-time systems (Zrenner et al., 2018). During wakefulness, real-time EEG-triggered TMS of M1 demonstrated phase-dependent MEP modulations during the sensorimotor mu-alpha rhythm (Bergmann et al., 2019; Zrenner et al., 2018), and TMS bursts repeatedly targeting the more excitable mu-alpha troughs induced long-term potentiation (LTP)-like MEP increases (Zrenner et al., 2018). While alpha amplitude modulations are slower and more easily predictable than spontaneous spindle bursts of the sigma band, spindles have a better signal-to-noise ratio (SNR).

Several automated offline spindle detection approaches are available (Lacourse et al., 2019; Parekh et al., 2017; Vallat & Walker, 2021; Warby et al., 2014; Weber, 2013), including machine or deep learning-based detection methods (Kaulen et al., 2022; Kulkarni et al., 2019; LaRocco et al., 2018) with a potential for real-time applications, but actual implementations are scarce. Lustenberger et al. (2016) used transcranial alternating current, while Antony et al. (2018) and Choi et al. (2019) used auditory stimulation to target ongoing spindles, but only basic information and no validation procedure was provided regarding the real-time algorithm and its phase specificity. The *Portiloop* system, a portable system on chip, at least achieved real-time spindle detection with an F1-Score of 71% by training artificial neural networks on a field-programmable gate array (Valenchon et al., 2021).

Here we present the real-time spindle detector (RTSD), a robust, empirically validated and fully automated real-time signal-processing algorithm that is able to identify spindles from ongoing EEG recordings close to their amplitude maximum (spindle centre) and send out a phase-specific trigger signal. We validated the RTSD using real-time streaming of pre-recorded sleep data from naps and full nights, comparing its performance with several state-of-the-art offline spindle detection algorithms, and evaluating key characteristics of the detected spindles.

2 | MATERIALS AND METHODS

2.1 | The RTSD

The RTSD identifies 0.5–2-s-long distinct oscillatory patterns of waxing and waning amplitude in the sigma band (12–15 Hz) in ongoing EEG data. Unlike offline algorithms that are "non-causal" (using data points from past, present and future) and can thus rely on long data segments comprising complete spindles, the RTSD has to work in a "causal" manner (including only past and present data points). To robustly detect spindles while they unfold and therefore with incomplete information about their final shape, duration and amplitude, the RTSD relies on the analysis of several complementary high-level signals derived from the raw data, which are evaluated in parallel and combined to make a decision (Figure 1). Also, personalized detection criteria related to individual spindle power and peak frequency cannot be taken from the full data of the same sleep recording but have to be derived from "baseline" sleep data, that is, a separate period of sleep EEG data recorded either during the beginning of the same sleep session or during a previous sleep session of the same subject (e.g. an adaptation night). In the latter case, spindle peak frequency and root mean square (RMS) of the spindle band power can be extracted using established offline detection procedures that utilize envelope-based detection, such as YASA, A7 or SpiSOP (Lacourse et al., 2019; Vallat & Walker, 2021; Weber, 2013).

2.1.1 | Hardware and software implementation

The RTSD algorithm is implemented in a real-time Simulink (MathWorks) environment in MATLAB r2017b, which can be compiled, loaded and run on any Simulink compatible real-time computer system. For actual real-time detection, digitized EEG/polysomnographic (PSG) data are streamed via a real-time compatible EEG amplifier with digital output streaming (e.g. NeurOne Tesla EEG system, Bittium, Finland or ActiChamp Plus, BrainProducts, Germany). For validation purposes in the present work, we replayed existing datasets to the compiled real-time Simulink model running on a dedicated real-time system (*bossdevice*, sync2brain Germany). The BEST toolbox (Hassan et al., 2022) was used to control the Simulink model, setting individual thresholds for spindle detection on the bossdevice. Raw time series data of the detected events, such as spindles and SOs as well as the instantaneous EEG phases at the time of detection, were recorded in data files for confirmatory post hoc offline analysis. In our implementation, the RTSD algorithm had a loop delay of 5–15 ms, which is induced primarily by the hardware, the interface software (here, Simulink) and the digital bandpass filters.

2.1.2 | Data preprocessing

Raw data can be processed through a number of custom spatial filters, that is, a linear combination of the streamed channels, resulting in an

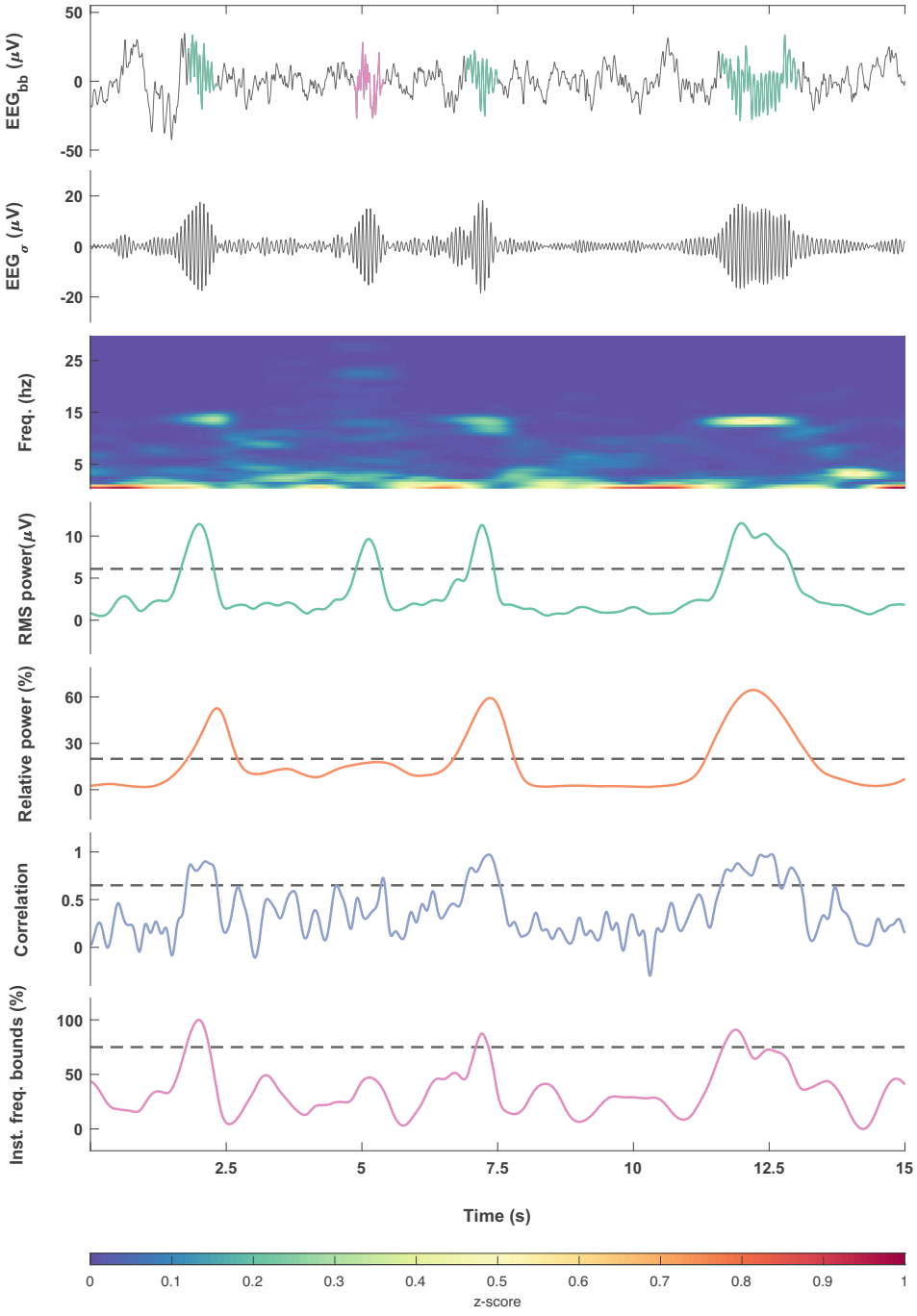

FIGURE 1 High-level signals computed by the real-time spindle detector (RTSD) algorithm. The RTSD computes several high-level signals, derived from the raw electroencephalographic (EEG) data of the virtual channel of interest (here electrode C3 re-referenced to right mastoid). Each dotted line represents the threshold for its respective high-level signal, that is: (i) EEG_{σ} RMS (root mean square) power; (ii) EEG_{σ} relative power; (iii) $EEG_{\sigma} \times EEG_{bb}$ correlation; and (iv) EEG_{bb} instantaneous frequency bounds. In the first row, the green shaded region represents detected spindle events, while the red shaded region represents a rejected non-spindle event that would have been a False Positive (FP) if based on the RMS power envelope alone

arbitrary number of virtual channels for which spindles can in principle be detected independently in parallel. However, a minimum of one virtual channel is required to detect spindles, for example, C3 re-referenced against the linked mastoids as used in our example for a typical use case. Every 10 ms, 520 ms of the most recent data are extracted and used for further analyses, resulting in a 98% overlap of consecutively extracted analysis windows. Then, by applying a two-pass (zero-phase) least-squares finite impulse response (FIR) filter of order 20 to the most recent 520-ms data segment we create two fundamental signals: using a passband of 1–30 Hz a broadband EEG signal (EEG_{bb}) is constructed; and using a passband of the individual spindle peak frequency ± 2 Hz a sigma band EEG signal (EEG_{σ}) is created. Then, 10 ms from each side of EEG_{bb} and EEG_{σ} is removed to create 500-ms segments of data that are free of filter edge artefacts. The filtered EEG_{bb} and EEG_{σ} signals are then further processed to derive four high-level signals, which are described in the following section together with their respective thresholds.

2.1.3 | Computation of high-level signals

EEG_{σ} RMS power signal

To gain an index of absolute spindle power, the RMS is computed using a 250-ms moving data window of EEG_{σ} with a step size of

100 ms to construct the EEG_{σ} RMS power signal. The RMS power threshold is individualized for each subject based on their baseline sleep data by taking the mean of the EEG_{σ} RMS power plus 1.5 times their SD.

EEG_{σ} relative power signal

To prevent broadband power changes from being mistaken for spindle-related increases in the sigma band, the EEG_{σ} RMS power signal needs to be normalized. A fast Fourier transform of the EEG_{bb} is used to calculate the EEG_{σ} relative power. A 500-ms moving data window is zero padded on both sides (250 ms each) to 1 s to construct a frequency spectrum with 1-Hz resolution. The power summed across the frequency bins corresponding to the spindle peak frequency ± 2 Hz (i.e. the individual sigma band) is divided by the power summed across the 1–30-Hz bins to construct the EEG_{σ} relative power signal. An increase in EEG_{σ} relative power is caused by a local increase in the power of the sigma band but not by broadband power increases that occur proportionally across the entire spectrum. A fixed threshold value of 15%–20% relative power is generally sufficient to estimate sigma-band-specific activity, but the threshold can also be determined individually based on the baseline sleep data.

$EEG_{\sigma} \times EEG_{bb}$ correlation signal

To prevent artefacts or noise in the raw data to be mistaken for actual spindle events in the sigma bandpass-filtered data, the actual waveform shape of the potential spindle is evaluated in the raw data. For this purpose, the Pearson correlation coefficient between EEG_{bb} and EEG_{σ} is calculated for a 250-ms moving data window. A high correlation coefficient indicates that the bandpass-filtered data reflect actual activity of the sigma band rather than artefacts or noise. A fixed threshold value of $r \geq 0.65$ is generally sufficient to detect N2 and N3 spindles, but the value may need to be adopted based on the SNR of spindles in the subject and the specific spatial filters applied.

EEG_{bb} instantaneous frequency signal

To further ensure the other high-level signals are not confounded by activity in neighbouring frequency bins (which for offline detection methods can be ensured by the use of higher-order bandpass filters), only spindle oscillations within certain frequency bounds are accepted. Therefore, the instantaneous frequency is calculated from the time derivative of the Hilbert phase of the EEG_{bb} signal over a 250-ms moving data window. Then, it is determined for which percentage of the data window the EEG_{bb} instantaneous frequency remains within the range of the individual spindle peak frequency ± 5 × the SD of the spindle frequency (Hz). A fixed threshold value of 75% generally indicates a stable instantaneous frequency in the sigma band.

2.1.4 | Spindle detection

Eventually, a spindle is detected when at least three out of the four above-described high-level signals satisfy their respective criteria and in addition the spindle duration criterion is met. This is the case when time since the EEG_{σ} RMS power signal crossed the "entry threshold" of mean + 1.15 SDs is greater than 250 ms, which corresponds to half of the minimum spindle duration of 500 ms, allowing for the identification of the spindle centre also for very short spindles. Maximum spindle power (i.e. the assumed spindle centre) is detected when the time derivative of the EEG_{σ} RMS power crosses zero and the RMS power begins to descend. The end of the spindle is detected once the signal falls below the "entry threshold" again. Spindle detection is suspended when the RMS power remains above the "entry threshold" for more than 2 s, and it resumes only after at least three of the four signals again exceed their respective thresholds.

2.1.5 | Real-time spindle phase estimation

In addition to detecting spindle events, also their oscillatory phase is estimated in real-time using the *phastimate* algorithm (Zrenner et al., 2020). In summary, the phase of the spatially filtered raw signal is continuously estimated by band-pass filtering the most recent 256-ms moving data window by a least-squares FIR filter with an order of 65 and a passband of the individual spindle frequency ± 2 Hz. Then, 32.5 ms on each side of the data segment is removed to create a data segment free of filter edge artefacts. The resulting 191-ms-long data segment is then used for 65-ms forward prediction using a Yule–Walker 15th order autoregressive model (Chen et al., 2013; McFarland & Wolpaw, 2008). The forward predicted 65-ms data segment provides ± 32.5 ms around time point zero. A fixed time offset equal to the software and hardware delays is then applied to the zero time point to identify the actual time point zero (i.e. "now"). A static range test is applied to the phase at this time point "now" obtained from the Hilbert phase time series of the forecasted signal to identify peaks, troughs, rising flanks and falling flanks. Phases estimated during the detected spindle event are considered spindle phases.

2.2 | Empirical validation of the RTSD

2.2.1 | Sleep EEG/PSG datasets

We validated our real-time algorithm in two independent datasets of EEG and PSG recordings from nocturnal naps (Dataset 1) and full nights (Dataset 2), respectively. *Dataset 1* consisted of $N = 20$ subjects (12 females, mean age: 23 ± 5 years) recorded during the stimulation-free adaptation session of an unpublished EEG-triggered TMS experiment conducted at the Neuroimaging Center (NIC) of the Johannes Gutenberg University Medical Center, Mainz. Subjects had no history of neurological or psychiatric disease, were right-handed, and did not take any medications. They were not allowed to drink alcohol or caffeine on the day of the experiment, and they had to be awake for at least 8 hr before the experiment to ensure moderate sleep pressure. Experimental procedures conformed to the

Declaration of Helsinki and were approved by the Ethics Committee of the Landesärztekammer Rheinland-Pfalz. EEG and PSG were recorded using a 64-channel EEG-cap with sintered Ag/AgCl electrodes (Multitrodes, EasyCap) containing the following electrodes according to 10–20 EEG system: Fp1, Fp2, Fpz, AF7, AF3, AFz, AF4, AF8, F7, F5, F3, F1, Fz, F2, F4, F6, F8, FT9, FT7, FC5, FC3, FC1, FC2, FC4, FC6, FT8, FT10, T7, C5, C3, C1, Cz, C2, C4, C6, T8, TP7, CP5, CP3, CP1, CPz, CP2, CP4, CP6, TP8, P7, P5, P3, P1, Pz, P2, P4, P6, P8, PO7, PO3, POz, PO4, PO8, O1, Oz, O2, M1 (left mastoid), M2 (right mastoid); Reference, FCz; Ground, POz. For PSG, electromyography (EMG) at the chin, and the vertical and horizontal electro-oculogram (VEOG and HEOG) were recorded using bipolar electrode montages. EEG and PSG data were digitized in DC mode with a 1250-Hz anti-aliasing low-pass filter and 5-kHz sampling rate using a TMS-compatible 24-bit amplifier (NeurOne Tesla with Digital-Out Option, Bittium) connected to an 8-V battery. The subjects slept in a sound-proof and electromagnetically shielded sleeping cabin (Desone, Germany) on a comfortable mattress resting on a wooden bed in a horizontal position. They were covered with a blanket and their heads were stabilized by a vacuum cushion. *Dataset 2* consisted of $N = 10$ subjects selected from the placebo session of a previously published study that examined the effects of blocking metabotropic glutamate receptor 5 on sleep-dependent memory consolidation (Feld et al., 2021). The data were collected at the sleep lab of the Institute of Medical Psychology and Behavioral Neurobiology, University of Tübingen, Germany. EEG and PSG were recorded using Ag/AgCl electrodes containing the following electrodes according to 10–20 EEG system: F4, Fz, F4, C3, Cz, C4, P3, Pz, P4; Referenced to linked mastoids; Ground electrode on the forehead. For PSG, EMG at the chin, and VEOG and HEOG were recorded using bipolar electrode montages. EEG and PSG data were digitized in DC mode with an 80-Hz low-pass filter and a sampling rate of 250 Hz. Further details regarding the sleep characteristics of all subjects are available in Tables S1 and S2.

2.2.2 | Detection criteria and offline spindle detection

We selected three previously published and frequently used offline spindle detection algorithms for comparison and validation of our RTSD method, namely YASA, A7 and SpiSOP. These offline algorithms are actively maintained as open-source software contributions, are well documented and are easy to use. Because the A7 spindle detector itself had been shown to outperform four previously published offline detection methods, namely Ferrarelli et al. (2007), Mölle et al. (2002), Martin et al. (2013) and Wamsley et al. (2012), we considered no further methods than the three mentioned ones for comparison. To ensure fair comparisons, the key spindle detection criteria for both our RTSD algorithm as well as all offline spindle detection algorithms were kept identical wherever possible, namely, to detect spindles in the 12–15-Hz frequency band, with a minimum duration of 0.5 s and maximum duration of 2 s, and an amplitude of mean + 1.5 times the SD of the RMS bandpass-filtered signal. Other RTSD-specific thresholds, that is, the EEG_{σ} relative power threshold, correlation threshold and instantaneous frequency bounds threshold, were fixed across all subjects at 20%, 0.65 and 75%, respectively. We used published software implementations of YASA (version 0.6.01) in Python release 3.10, and of A7 (version 1.1.2) and SpiSOP in MATLAB r2017b.

For comparison with our real-time spindle algorithm, we selected channel C3 from Dataset 1 (nap recordings) re-referenced against the average of both mastoids. For Dataset 2 (full-night recordings), we selected channel C3, already referenced against a linked mastoids during the original recordings. Additionally, EMG, HEOG and VEOG from PSG were selected and used in the automatic sleep scoring implemented in YASA. To separate the effect of the different spindle detection algorithms from the potential impact of the sleep scoring, spindle detection was performed twice, once on the entire data irrespective of sleep stage, and once restricted to sleep stages N2 and N3 as obtained from YASA automated sleep stage scoring. YASA scoring results were used for all validation runs with offline algorithms as well as the RTSD algorithm. For the naps of Dataset 1, a manual check of the automatic sleep stage scoring was performed for quality control as recommended for naps in the YASA software.

2.2.3 | Performance assessment

We assessed the performance of the RTSD against each of the offline spindle detectors, using the respective offline algorithm as ground truth. Specifically, we assessed the number of correct spindle detections (True Positive; TP), of incorrect spindle detections (False Positive; FP) and of missed spindles (False Negative; FN). Correct rejections (True Negatives; TN) cannot reasonably be assessed for rare events in continuous data and are therefore not provided. Using the method of intersection (Lacourse et al., 2019; LaRocco et al., 2018; Warby et al., 2014), the ratio between the intersection and union of the respectively detected spindle intervals was calculated for each spindle, and a spindle match (TP) was determined whenever the ratio was greater than 0.2. Unmatched spindles found in the offline detectors were categorized as FN, and unmatched spindles found in the real-time detector were categorized as FP. Based on these numbers, we determined Sensitivity (i.e. the percentage of detected spindles that are true spindles), Precision (i.e. the percentage of true spindles that are detected spindles) and the F1-Score (an established compound index for assessing detection algorithms combining Sensitivity and Precision) as defined below:

$$\text{Sensitivity} = \frac{TP}{TP + FN} \quad (1)$$

$$\text{Precision} = \frac{TP}{TP + FP} \quad (2)$$

$$\text{F1} - \text{Score} = 2 \times \frac{\text{Precision} \times \text{Sensitivity}}{\text{Precision} + \text{Sensitivity}} \quad (3)$$

The RTSD was compared with YASA, A7 and SpiSOP. As a benchmark for the maximally expected levels of Sensitivity, Precision and

F1-Score, all three state-of-the-art offline detectors were also tested against each other, resulting in a total of six different comparisons (real-time versus YASA; real-time versus A7; real-time versus SpiSOP; YASA versus A7; YASA versus SpiSOP; and A7 versus SpiSOP).

To further characterize the spindles detected in real-time: (i) morphological properties of the detected spindles, such as spindle frequency, amplitude, duration and symmetry of wave shape, were calculated and compared with offline detected spindles as described by Purcell et al. (2017); (ii) time–frequency representations (TFRs) were calculated to verify their typical narrow-band waxing and waning pattern; and (iii) topographical representations of spindle power were plotted to verify their distinct localization with respect to the EEG montage selected for detection.

Time–frequency analysis of spindle-related oscillatory power changes was carried out using the FieldTrip toolbox (Oostenveld et al., 2011). For all spindles, raw spatially filtered data segments of −1 to 1 s around the real-time detected spindle centre were retrieved from the real-time system (bossdevice). Data were then preprocessed by de-meaning and a 1-Hz high-pass filter. TFRs were calculated separately for TP and FP spindles (compared against YASA) by using a Hanning taper windowed FFT (time steps: 50 ms; frequency steps: 0.5 Hz). TFRs were plotted as percentage power change relative to the full epoch of −1 to 1 s as baseline. Sigma power topographies were plotted for the time interval of −500 to 500 ms as the percentage change in power from the baseline at −550 to −500 ms.

To test whether spindle phase targeting worked as expected, spindle phase was additionally validated with the phase-detection module enabled and four different spindle phase targets (peak, falling flank, trough and rising flank) in four additional detection runs: post hoc we determined the actual phase of the trigger signal based on the Hilbert transform of the sigma bandpass-filtered (individual sigma peak ± 2 Hz) EEG signal, and evaluated the phase targeting precision using the circular SD method of CircStat toolbox (Berens, 2009).

3 | RESULTS

3.1 | Performance of RTSD is comparable to offline algorithms

When limiting spindle detection to NREM epochs, the following performance indices were obtained. The grand average F1-Score for RTSD versus the different offline algorithms was 78%–84% (compared with 80%–81% between the offline algorithms) for the naps, and 79%–83% (compared with 81% between the offline algorithms) for the full-nights. The grand average Sensitivity for RTSD versus the different offline algorithms was 80%–87% (compared with 83%–85% between the offline algorithms) for the naps, and 81%–86% (compared with 83%–86% between the offline algorithms) for the full-nights. The grand average Precision for RTSD versus the different offline algorithms was 76%–80% (compared with 77%–78% between the offline algorithms) for the naps, and 78%–81% (compared with 78%–80% between the offline algorithms) for the full-nights (see Table 1 for all grand average values, and Figure 2 for distributions and subject-wise performance indices). When spindles were identified without limiting the search of the algorithms to NREM sleep stages, Sensitivity, Precision and F1-Scores were overall slightly reduced for both naps and full-night recordings, but still better for comparisons between RTSD and offline detection than between the offline

TABLE 1 Grand average values of performance characteristics in percent (%)

	RTSD versus YASA	RTSD versus A7	RTSD versus SpiSOP	YASA versus A7	YASA versus SpiSOP	A7 versus SpiSOP
Spindle detection restricted to NREM sleep epochs						
F1-Score (nap)	84 ± 3	79 ± 3	78 ± 5	80 ± 2	80 ± 3	81 ± 2
Sensitivity (nap)	87 ± 5	83 ± 4	80 ± 5	84 ± 3	83 ± 3	85 ± 4
Precision (nap)	80 ± 4	76 ± 5	77 ± 3	77 ± 4	78 ± 2	78 ± 4
F1-Score (full-night)	83 ± 4	80 ± 2	79 ± 4	81 ± 3	81 ± 2	81 ± 2
Sensitivity (full-night)	86 ± 6	81 ± 5	81 ± 6	84 ± 4	86 ± 5	83 ± 5
Precision (full-night)	81 ± 5	78 ± 4	78 ± 4	79 ± 3	78 ± 3	80 ± 4
Spindle detection not restricted by sleep stage information						
F1-Score (nap)	73 ± 6	69 ± 5	69 ± 7	64 ± 5	63 ± 4	63 ± 6
Sensitivity (nap)	74 ± 5	71 ± 6	69 ± 7	66 ± 5	65 ± 6	65 ± 5
Precision (nap)	72 ± 5	67 ± 5	69 ± 5	62 ± 6	62 ± 4	61 ± 6
F1-Score (full-night)	71 ± 6	70 ± 6	69 ± 6	63 ± 5	64 ± 6	64 ± 5
Sensitivity (full-night)	71 ± 7	72 ± 5	68 ± 7	65 ± 6	66 ± 6	65 ± 5
Precision (full-night)	70 ± 6	68 ± 6	69 ± 5	60 ± 5	60 ± 5	62 ± 6

Means (± SD) are reported.
Abbreviations: NREM, non-rapid eye movement; RTSD, real-time spindle detector.

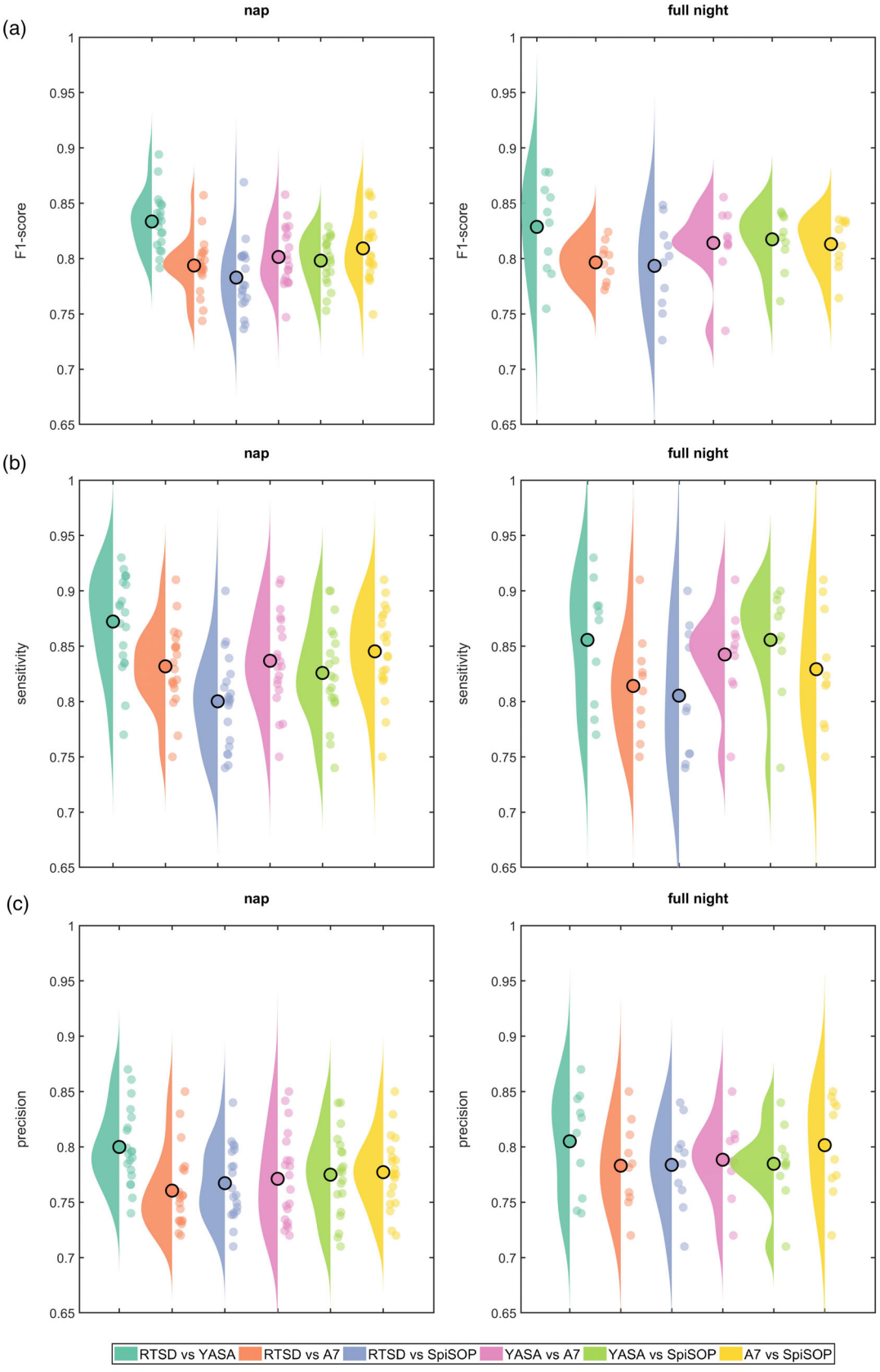

FIGURE 2 Performance values for comparisons of real-time spindle detector (RTSD) and offline algorithms including non-rapid eye movement (NREM) sleep epochs only. RTSD was compared against offline algorithms (YASA, A7 and SpiSOP) and in between offline algorithms for the nap recordings (dataset 1) and full-night recordings (dataset 2) for: (a) F1-Scores; (b) Sensitivity; and (c) Precision. Single-subject data points (coloured filled circles) and raincloud plots are provided in addition to the condition mean (black open circle)

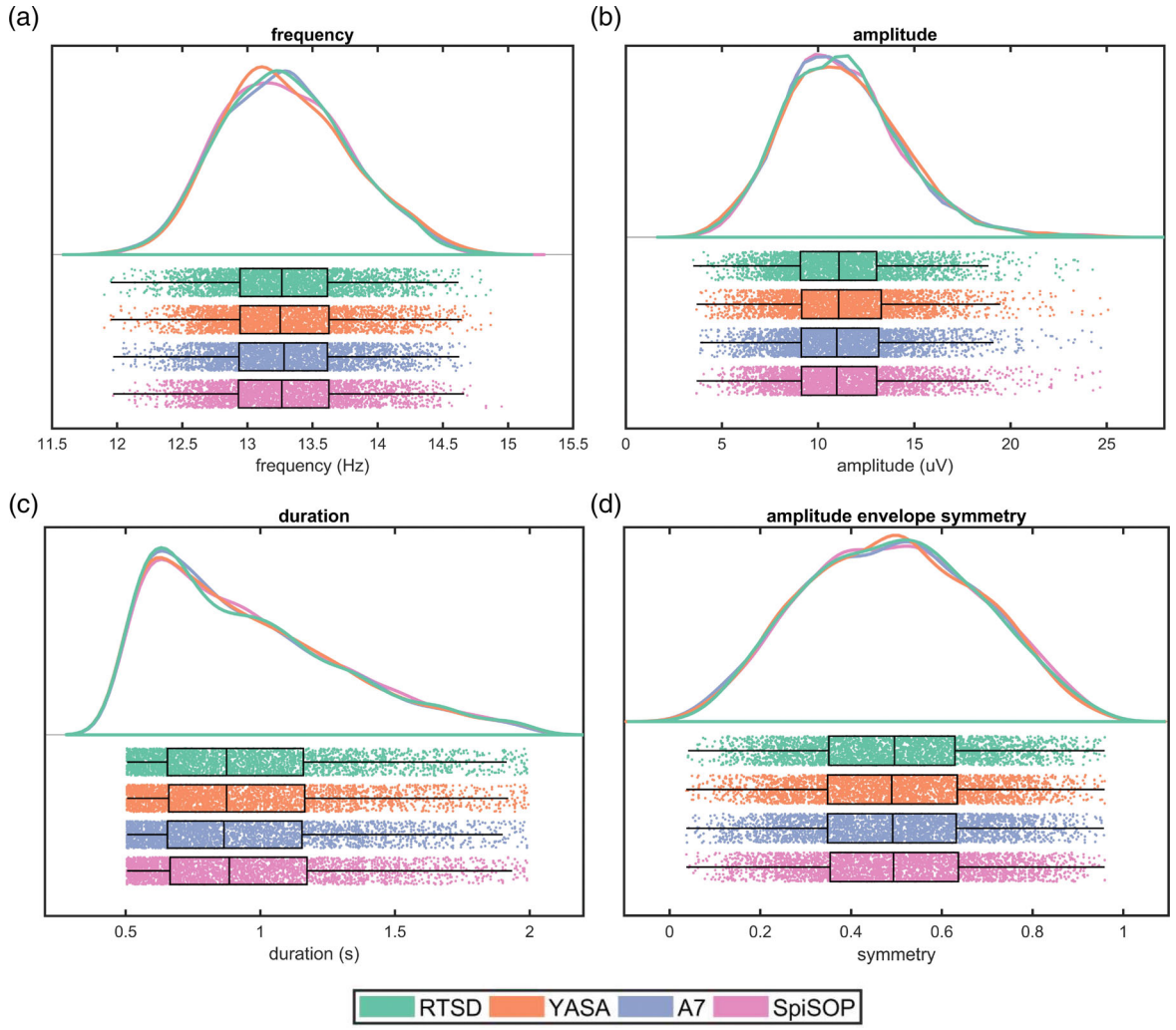

FIGURE 3 Morphological properties of real-time and offline detected spindles. Distributions across all detected spindles of all subjects and data points of all individual spindles events are provided for morphological spindle traits extracted by the same procedure, being highly comparable with respect to: (a) frequency (Hz); (b) amplitude (μV); (c) duration (s); and (d) symmetry index of the spindle amplitude envelope

detectors themselves when providing no sleep staging information (Figure S1; Table 1).

3.2 | Properties of real-time detected spindles are comparable to those detected offline

When comparing the distributions of spindle frequency, amplitude, duration and symmetry of the spindle amplitude envelope for the events detected by the RTSD and the different offline algorithms (confined to NREM sleep epochs), highly similar distributions were obtained (Figure 3), confirming the high contingency levels described above and no systematic differences in the type of spindles being detected.

TFRs (Figure 4a) and topographical distribution of sigma power (Figure 4b) of TP spindles detected using RTSD revealed that the TP spindles (here defined in comparison to YASA) were detected as intended, and that neither adjacent frequencies nor oscillatory activity from other sources had confounded the RTSD procedure.

3.3 | Spindle phase targeting was reliable

To verify that the instantaneous oscillatory phase of an ongoing spindle can be reliably determined in real-time, we confirmed the phase targeting post hoc by extracting the phase information from the Hilbert transform of the individual sigma bandpass-filtered signal. We did this separately for the four target phases (peak, trough, rising flank, falling flank), but collapsed across both datasets while including only periods of NREM sleep (Figure 5). All spindle phases were correctly targeted with an average circular SD of 53.4° across all phase angles (peak: 53.9°; falling flank: 55.1°; trough: 54.6°; rising flank: 50.2°).

4 | DISCUSSION

We have presented and validated a novel method for robustly detecting sleep spindles automatically in real-time. The RTSD identifies ongoing spindle activity by transforming the raw EEG in several high-level signals that are evaluated in parallel, and then detecting spindle

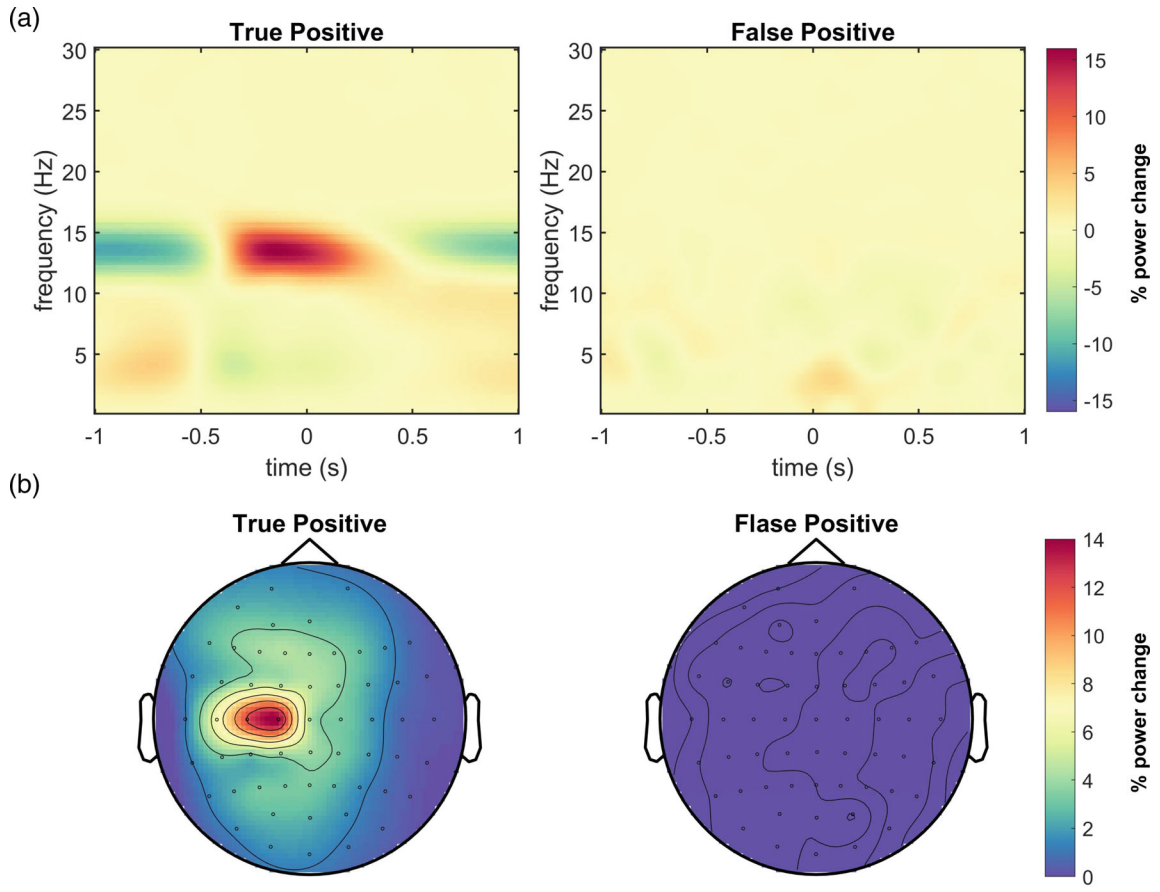

FIGURE 4 Topographical distribution and time–frequency representation (TFR) of real-time detected spindles. (a) TFRs of oscillatory power in the C3 signal re-referenced against linked mastoids, calculated separately for real-time spindle detector (RTSD) detected True Positive (TP) and RTSD False Positive (FP) spindles (as compared with YASA) with a baseline interval of −1 to 1 s. TFRs of TP spindles show a modulation of sigma power over time, with a relative increase from −500 ms to 500 ms around spindle centre and relative decrease before −500 ms and after 500 ms. FP spindles showed no particular pattern in the TFR that would be indicative of a particular temporal or frequency source of electroencephalographic (EEG) signals leading to false alarms. (b) Topographical maps of the sigma power modulation from −500 ms to 500 ms (taken from a) for TP and FP spindles detected by RTSD with a baseline interval of −550 ms to −500 ms. The topography of TP spindles verifies a local sigma power increase over C1 to C3 (specific to the target montage), suggesting that also local spindles can be targeted using RTSD. FP spindles showed no particular topography that would be indicative of a particular spatial source of EEG signals leading to false alarms

activity in one or more EEG channels in a manner similar to offline spindle detection.

The performance of the RTSD was very good (F1-Score about 0.8), with well-balanced Sensitivity and Precision levels. Higher levels were not to be expected, given that the automatic offline detection algorithms themselves did not reach higher levels when compared with each other. The F1-Scores reported for other offline spindle detection methods are even slightly lower, for example, A7 scored at 0.72 (Lacourse et al., 2019), DETOKS at 0.67 (Parekh et al., 2015), Spindler at 0.67 (LaRocco et al., 2018) and Spinky at 0.74 (Lajnef et al., 2017). However, the lower F1-Scores may also be caused by the fact that these offline methods used expert labelled data as ground truth, whereas we used automatic offline spindle detectors. In addition, these methods detected spindles as short as 300 ms rather than 500 ms, which is slightly easier to detect by automated detection techniques. We deliberately used multiple established state-of-the-art offline spindle detection algorithms as ground truths instead of manual expert ratings, because the RTSD algorithm is not meant to compete with clinical sleep scoring procedures but to provide a novel method for neuroscientific research into the function of sleep spindles using sensory and transcranial brain stimulation approaches, for which the approximation of human judgements is less important than the use of objective and reproducible criteria. If desired, changing RTSD detection criteria allows for a flexible adjustment of Sensitivity versus Precision, to be as liberal or as conservative as required by the experimental design and research question.

Performance indicators were reduced only slightly for RTSD (by ~10%) when spindle detection was not restricted to NREM sleep stages, while larger drops were observed in the consistency between offline algorithms (by ~15%–20%; Figure S1; Table 1). This shows that while sleep stage information improves the F1-Score, the RTSD is very robust and can also be used in real-time detection settings where no sleep scoring information is available during the ongoing recordings. This robustness is remarkable, given that the RTSD has to

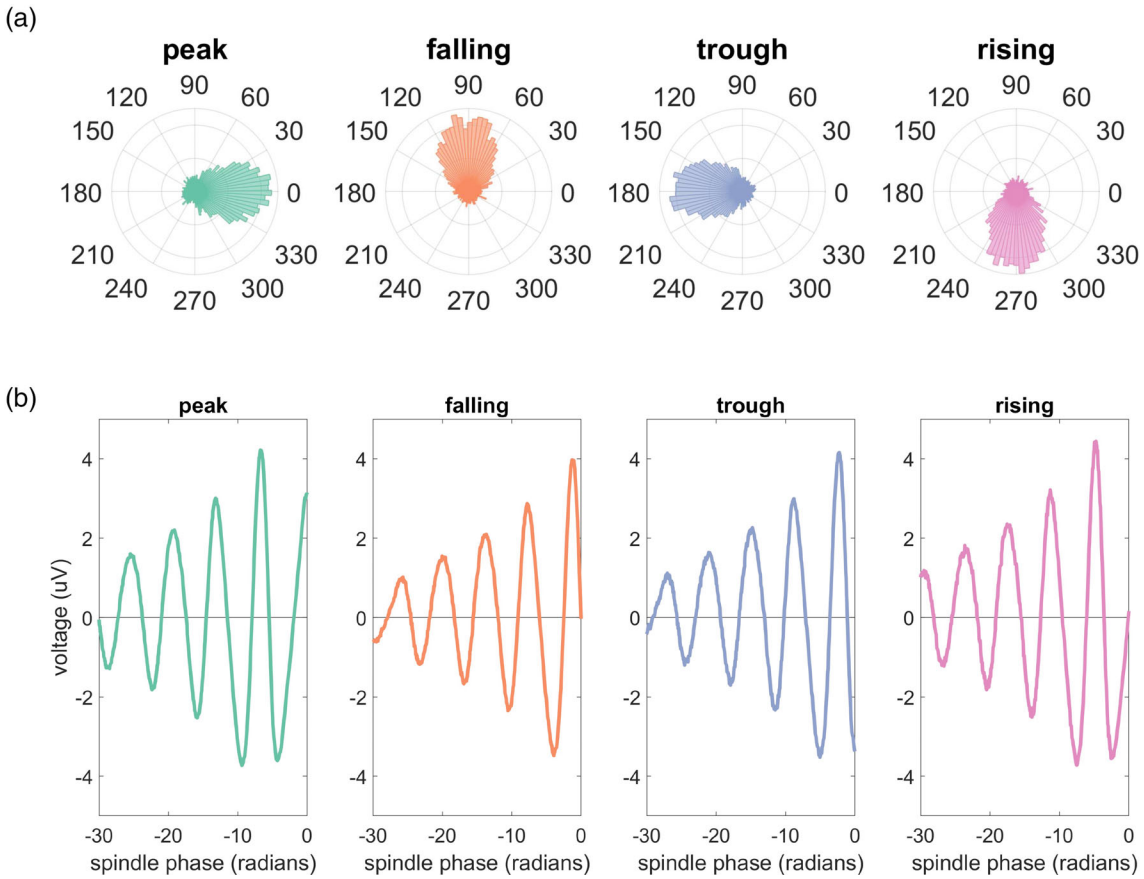

FIGURE 5 Phase estimates for different phase targets during spindles. (a) Phase histograms of all spindles that were detected time-locked to each of the four explicit phase targets (peak, falling flank, trough, rising flank). Actual phase angles were determined post hoc using the Hilbert transform. (b) Time-locked C3 signal re-referenced against linked mastoids with the time axis transformed to phase angles (radians) of the individual spindle peak frequency before averaging across subjects to account for inter-individual differences in frequency. Spindle phase detection was successfully time locked to peaks, falling flanks, troughs and rising flanks

work on less information (data) than the offline algorithms. A7, YASA and SpiSOP require data segments of at least a few seconds to identify complete spindles, whereas the RTSD method only uses the most recent 500 ms and per definition only the first half of the ongoing spindle for detection. However, the RTSD compensates the lack of temporal information by the parallel assessment of several high-level signals derived from the incoming raw data. For example, none of the offline methods assesses whether the instantaneous frequency is within the desired bounds, which constitutes one of the four key thresholds in RTSD.

The primary limitation of the RTSD is that it locates the spindle centre by detecting zero crossings of the amplitude envelope derivative as soon as the envelope begins to descend, while in reality spindle amplitude envelopes can have more than one maximum. The RTSD only detects local maxima following 250 ms of spindle onset (i.e. since the envelope has crossed the "entry threshold"), regardless of whether this is a global maxima. Together with the loop delay of 5–15 ms reached in our implementation (Simulink® Real-Time™ on a bossdevice from sync2brain), spindles cannot be targeted during their initial waxing phase. Removing the criterion of detecting a spindle centre may allow earlier targets within a spindle but will also increase the false-positive rate; whether or not this is acceptable eventually depends on the study goals. This limitation may also be overcome in the future by using additional information from the data (such as power envelope gradients) or by training deep learning approaches to predict spindles during very early phases or even before their initiation (Valenchon et al., 2021).

Using the RTSD default threshold settings, the detected spindles expressed morphological traits very similar to those detected by the offline algorithms. Moreover, TFRs of the TP spindles confirmed the typical pattern of a time-limited narrow sigma band frequency increase during the spindle preceded and followed by relative decreases, which may reflect the influence of a phase-amplitude modulating SO. False-positive spindles were not associated with any particular time–frequency pattern, indicating that there was no particular systematic temporal or frequency source of EEG signals leading to false alarms. Topographical sigma power maps of TP spindles showed the typical central topography of sleep spindles, but with a lateralization towards the left hemisphere (peaking at channel C1 and extending to C3), which is presumably owed to the left-lateralized montage

(C3 versus linked mastoids) used for spindle detection in our validation runs. Again, FP spindles did not show a systematic sigma power distribution, indicating that no particular spatial source of EEG signals led to false alarms. Together, these auxiliary analyses confirm that the RTSD algorithm can effectively detect true sleep spindles that are very comparable to those detected by offline algorithms, without a systematic source of false alarms.

The RTSD algorithm allows targeting spindles in a phase- and amplitude-dependent manner to study the neurophysiological underpinnings of this important oscillation as well as its role in sleep-dependent memory reactivation and consolidation, using either non-invasive brain stimulation (like TMS) or sensory stimulation (such as auditory or somatosensory stimuli). Just like for mu-alpha oscillations during wakefulness (Bergmann et al., 2019; Zrenner et al., 2018), spindle phase-dependent single- and paired-pulse TMS can be used to characterize amplitude- and phase-dependent modulations of cortical excitability and excitation–inhibition balance. Using MEPs and TMS-evoked EEG potentials as indices of cortical excitability and network responsivity without changing the spindle itself by the stimulation, this approach qualifies as open-loop brain-state-dependent stimulation (OL-BSDS). Similarly, phase-triggered repetitive TMS protocols can induce after-effects in cortical excitability outlasting the stimulation period (Ziemann et al., 2008), presumably related to phase-dependent long-term potentiation (LTP)- and long-term depotentation (LTD)-like plasticity (Bergmann & Born, 2018), an OL-BSDS approach that may help to uncover the role of spindles in synaptic plasticity. Moreover, spindle (phase)-triggered TMS bursts may also interfere with local or network events of memory reactivation allowing researchers to study their causal relevance for systems consolidation of memory. Finally, also fully closed-loop brain-state-dependent stimulation (CL-BSDS) protocols can be developed. The envisioned CL-BSDS protocols may allow to entrain or even up- and downregulate spindle activity to modulate associated processes of memory reactivation and consolidation more effectively, as TMS or auditory stimuli would not only be applied at spindle frequency (Antony & Paller, 2017; Ngo et al., 2019) in an open-loop brain-state-independent (OL-BSIS) fashion but synchronized to specific phase angles of spontaneously occurring spindles. Sleep spindle-triggered brain stimulation has thus a potential to contribute to our understanding of the neural mechanisms underlying synaptic plasticity and memory during sleep, and may thus even set the stage for therapeutic applications in neurorehabilitation or for alleviating memory impairments in neuropsychiatric conditions.

5 | CONCLUSION

We have proposed and validated the RTSD, an automated real-time sleep spindle detection method working on single- or multiple-channel montages in parallel to robustly identify sleep spindles in digitally streamed EEG data. A comparison between RTSD and several state-of-the-art offline spindle detection algorithms using data from both naps and full nights of sleep revealed that RTSD performed at least as well as the offline methods, even in the absence of sleep stage information. The RTSD method therefore holds significant potential for use with real-time EEG-triggered sensory or transcranial brain stimulation to study sleep-dependent memory consolidation or synaptic plasticity in humans.

AUTHOR CONTRIBUTIONS

Umair Hassan and Til Ole Bergmann conceptualized the study. Gordon B. Feld provided validation data. Umair Hassan designed, developed and tested the algorithm; Umair Hassan and Til Ole Bergmann wrote the manuscript; all authors jointly discussed and revised the manuscript.

ACKNOWLEDGEMENTS

This work was supported by funding from the Boehringer Ingelheim Foundation (BIF) and the German Research Foundation (DFG Grant 362546008) to Til Ole Bergmann. Open Access funding enabled and organized by Projekt DEAL.

CONFLICT OF INTEREST

Umair Hassan is head of software development at sync2brain GmbH, Germany. Other authors declare no competing financial interests. The other authors declare no conflicts of interest.

DATA AVAILABILITY STATEMENT

Data available on request from the authors.

ORCID

Umair Hassan https://orcid.org/0000-0001-8245-0061

REFERENCES

Antony, J. W., & Paller, K. A. (2017). Using oscillating sounds to manipulate sleep spindles. *Sleep*, *40*(3), zsw068. https://doi.org/10.1093/sleep/zsw068

Antony, J. W., Piloto, L., Wang, M., Pacheco, P., Norman, K. A., & Paller, K. A. (2018). Sleep spindle refractoriness segregates periods of memory reactivation. *Current Biology*, *28*(11), 1736–1743.

Berens, P. (2009). CircStat: A MATLAB toolbox for circular statistics. *Journal of Statistical Software*, *31*, 1–21.

Bergmann, T. O. (2018). Brain state-dependent brain stimulation. *Frontiers in Psychology*, *9*, 2108. https://doi.org/10.3389/fpsyg.2018.02108

Bergmann, T. O., & Born, J. (2018). Phase-amplitude coupling: A general mechanism for memory processing and synaptic plasticity? *Neuron*, *97*(1), 10–13.

Bergmann, T. O., Lieb, A., Zrenner, C., & Ziemann, U. (2019). Pulsed facilitation of corticospinal excitability by the sensorimotor mu-alpha rhythm. *The Journal of Neuroscience*, *39*(50), 10034–10043. https://doi.org/10.1523/JNEUROSCI.1730-19.2019

Bergmann, T. O., Mölle, M., Diedrichs, J., Born, J., & Siebner, H. R. (2012). Sleep spindle-related reactivation of category-specific cortical regions after learning face-scene associations. *NeuroImage*, *59*(3), 2733–2742.

Bergmann, T. O., Mölle, M., Schmidt, M. A., Lindner, C., Marshall, L., Born, J., & Siebner, H. R. (2012). EEG-guided transcranial magnetic stimulation reveals rapid shifts in motor cortical excitability during the human sleep slow oscillation. *Journal of Neuroscience*, *32*(1), 243–253.

Chen, W. M., Chiueh, H., Chen, T. J., Ho, C. L., Jeng, C., Ker, M. D., Lin, C. Y., Huang, Y. C., Chou, C. W., Fan, T. Y., Cheng, M. S., Hsin, Y. L., Liang, S. F., Wang, Y. L., Shaw, F. Z., Huang, Y. H., Yang, C. H., & Wu, C. Y. (2013). A fully integrated 8-channel closed-

loop neural-prosthetic CMOS SoC for real-time epileptic seizure control. *IEEE Journal of Solid-State Circuits*, *49*(1), 232–247.

Choi, J., Won, K., & Jun, S. C. (2019). Acoustic stimulation following sleep spindle activity may enhance procedural memory consolidation during a nap. *IEEE Access*, *7*, 56297–56307.

Diekelmann, S., & Born, J. (2010). The reminiscence perform of sleep. *Nature Reviews. Neuroscience*, *11*(2), 114–126.

Feld, G. B., Bergmann, T. O., Alizadeh-Asfestani, M., Stuke, V., Wriede, J. P., Soekadar, S., & Born, J. (2021). Specific changes in sleep oscillations after blocking human metabotropic glutamate receptor 5 in the absence of altered memory function. *Journal of Psychopharmacology*, *35*(6), 652–667.

Ferrarelli, F., Huber, R., Peterson, M. J., Massimini, M., Murphy, M., Riedner, B. A., Watson, A., Bria, P., & Tononi, G. (2007). Reduced sleep spindle activity in schizophrenia patients. *American Journal of Psychiatry*, *164*(3), 483–492.

Göldi, M., van Poppel, E. A. M., Rasch, B., & Schreiner, T. (2019). Increased neuronal signatures of targeted memory reactivation during slow-wave up states. *Scientific Reports*, *9*, 2715.

Hassan, U., Pillen, S., Zrenner, C., & Bergmann, T. O. (2022). The brain electrophysiological recording & stimulation (BEST) toolbox. *Brain Stimulation*, *15*(1), 109–115.

Kaulen, L., Schwabedal, J. T., Schneider, J., Ritter, P., & Bialonski, S. (2022). Advanced sleep spindle identification with neural networks. *Scientific Reports*, *12*(1), 1–10.

Klinzing, J. G., Niethard, N., & Born, J. (2019). Mechanisms of systems memory consolidation during sleep. *Nature Neuroscience*, *22*, 1598–1610.

Kulkarni, P. M., Xiao, Z., Robinson, E. J., Jami, A. S., Zhang, J., Zhou, H., Henin, S. E., Liu, A. A., Osorio, R. S., Wang, J., & Chen, Z. (2019). A deep learning approach for real-time detection of sleep spindles. *Journal of Neural Engineering*, *16*(3), 036004.

Lacourse, K., Delfrate, J., Beaudry, J., Peppard, P., & Warby, S. C. (2019). A sleep spindle detection algorithm that emulates human expert spindle scoring. *Journal of Neuroscience Methods*, *316*, 3–11.

Lajnef, T., O'Reilly, C., Combrisson, E., Chaibi, S., Eichenlaub, J. B., Ruby, P. M., Aguera, P.-E., Samet, M., Kachouri, A., Frenette, S., Carrier, J., & Jerbi, K. (2017). Meet spinky: An open-source spindle and K-complex detection toolbox validated on the open-access Montreal archive of sleep studies (MASS). *Frontiers in Neuroinformatics*, *11*, 15.

LaRocco, J., Franaszczuk, P. J., Kerick, S., & Robbins, K. (2018). Spindler: A framework for parametric analysis and detection of spindles in EEG with application to sleep spindles. *Journal of Neural Engineering*, *15*(6), 66015.

Lustenberger, C., Boyle, M. R., Alagapan, S., Mellin, J. M., Vaughn, B. V., & Fröhlich, F. (2016). Feedback-controlled transcranial alternating current stimulation reveals a functional role of sleep spindles in motor memory consolidation. *Current Biology*, *26*(16), 2127–2136.

Martin, N., Lafortune, M., Godbout, J., Barakat, M., Robillard, R., Poirier, G., Bastien, C., & Carrier, J. (2013). Topography of age-related changes in sleep spindles. *Neurobiology of Aging*, *34*(2), 468–476.

McFarland, D. J., & Wolpaw, J. R. (2008). Sensorimotor rhythm-based brain–computer interface (BCI): Model order selection for autoregressive spectral analysis. *Journal of Neural Engineering*, *5*(2), 155–162.

Mölle, M., Marshall, L., Gais, S., & Born, J. (2002). Grouping of spindle activity during slow oscillations in human non-rapid eye movement sleep. *Journal of Neuroscience*, *22*(24), 10941–10947.

Ngo, H., Miedema, A., Faude, I., Martinetz, T., Mölle, M., & Born, J. (2015). Driving sleep slow oscillations by auditory closed-loop stimulation--a self-limiting process. *Journal of Neuroscience*, *35*(17), 6630–6638.

Ngo, H. V., Martinetz, T., Born, J., & Molle, M. (2013). Auditory closed-loop stimulation of the sleep slow oscillation enhances memory. *Neuron*, *78*(3), 545–553. https://doi.org/10.1016/j.neuron.2013.03.006

Ngo, H. V., Seibold, M., Boche, D. C., Molle, M., & Born, J. (2019). Insights on auditory closed-loop stimulation targeting sleep spindles in slow oscillation up-states. *Journal of Neuroscience Methods*, *316*, 117–124. https://doi.org/10.1016/j.jneumeth.2018.09.006

Oostenveld, R., Fries, P., Maris, E., & Schoffelen, J. M. (2011). FieldTrip: Open source software for advanced analysis of MEG, EEG, and invasive electrophysiological data. *Computational Intelligence and Neuroscience*, *2011*, 156869.

Parekh, A., Selesnick, I. W., Osorio, R. S., Varga, A. W., Rapoport, D. M., & Ayappa, I. (2017). Multichannel sleep spindle detection using sparse low-rank optimization. *Journal of Neuroscience Methods*, *288*, 1–16.

Parekh, A., Selesnick, I. W., Rapoport, D. M., & Ayappa, I. (2015). Detection of K-complexes and sleep spindles (DETOKS) using sparse optimization. *Journal of Neuroscience Methods*, *251*, 37–46.

Purcell, S. M., Manoach, D. S., Demanuele, C., Cade, B. E., Mariani, S., Cox, R., Panagiotaropoulou, G., Saxena, R., Pan, J. Q., Smoller, J. W., Redline, S., & Stickgold, R. (2017). Characterizing sleep spindles in 11,630 individuals from the National Sleep Research Resource. *Nature Communications*, *8*(1), 1–16.

Shimizu, R. E., Connolly, P. M., Cellini, N., Armstrong, D. M., Hernandez, L. T., Estrada, R., Aguilar, M., Weisend, M. P., Mednick, S. C., & Simons, S. B. (2018). Closed-loop targeted memory reactivation during sleep improves spatial navigation. *Frontiers in Human Neuroscience*, *12*, 28.

Staresina, B. P., Bergmann, T. O., Bonnefond, M., van der Meij, R., Jensen, O., Deuker, L., Elger, C. E., Axmacher, N., & Fell, J. (2015). Hierarchical nesting of slow oscillations, spindles and ripples in the human hippocampus during sleep. *Nature Neuroscience*, *18*(11), 1679–1686.

Valenchon, N., Bouteiller, Y., Jourde, H. R., Coffey, E. B. J., & Beltrame, G. (2021). The Portiloop: A deep learning-based open science tool for closed-loop brain stimulation. *PLoS One*, *17*, e0270696. https://doi.org/10.48550/arXiv.2107.13473

Vallat, R., & Walker, M. P. (2021). An open-source, high-performance tool for automated sleep staging. *eLife*, *10*, e70092.

Wamsley, E. J., Tucker, M. A., Shinn, A. K., Ono, K. E., McKinley, S. K., Ely, A. V., Goff, D. C., Stickgold, R., & Manoach, D. S. (2012). Reduced sleep spindles and spindle coherence in schizophrenia: Mechanisms of impaired memory consolidation? *Biological Psychiatry*, *71*(2), 154–161.

Warby, S. C., Wendt, S. L., Welinder, P., Munk, E. G., Carrillo, O., Sorensen, H. B., Jennum, P., Peppard, P. E., Perona, P., & Mignot, E. (2014). Sleep-spindle detection: Crowdsourcing and evaluating performance of experts, non-experts and automated methods. *Nature Methods*, *11*(4), 385–392.

Weber, F (2013). SpiSOP, RRID:SCR_015673.

Ziemann, U., Paulus, W., Nitsche, M. A., Pascual-Leone, A., Byblow, W. D., Berardelli, A., Siebner, H. R., Classen, J., Cohen, L. G., & Rothwell, J. C. (2008). Consensus: Motor cortex plasticity protocols. *Brain Stimulation*, *1*(3), 164–182.

Zrenner, C., Desideri, D., Belardinelli, P., & Ziemann, U. (2018). Real-time EEG-defined excitability states determine efficacy of TMS-induced plasticity in human motor cortex. *Brain Stimulation*, *11*, 374–389.

Zrenner, C., Galevska, D., Nieminen, J. O., Baur, D., Stefanou, M. I., & Ziemann, U. (2020). The shaky ground truth of real-time phase estimation. *NeuroImage*, *214*, 116761.

SUPPORTING INFORMATION

Additional supporting information can be found online in the Supporting Information section at the end of this article.

How to cite this article: Hassan, U., Feld, G. B., & Bergmann, T. O. (2022). Automated real-time EEG sleep spindle detection for brain-state-dependent brain stimulation. *Journal of Sleep Research*, *31*(6), e13733. https://doi.org/10.1111/jsr.13733